Journal of the European Ceramic Society 42 (2022) 1963–1970

Contents lists available at ScienceDirect

Journal of the European Ceramic Society

journal homepage: www.elsevier.com/locate/jeurceramsoc

Original Article

Multiscale 2D/3D microshaping and property tuning of polymer-derived SiCN ceramics

Lorenz Hagelüken [a,*], Pradeep Vallachira Warriam Sasikumar [b], Ho-Yun Lee [a], David Di Stadio [a], Yashoda Chandorkar [c], Markus Rottmar [c], Katharina Maniura-Weber [c], Gurdial Blugan [b], Juergen Brugger [a,*]

[a] Microsystems Laboratory, Ecole Polytechnique Fédérale de Lausanne, 1015 Lausanne, Switzerland
[b] Laboratory of High Performance Ceramics, Empa, Swiss Federal Laboratories for Material Science and Technology, 8600 Dübendorf, Switzerland
[c] Laboratory for Biointerfaces, Empa, Swiss Federal Laboratories for Material Science and Technology, 9014 St. Gallen, Switzerland

ARTICLE INFO

Keywords:
Polymer-derived ceramics
Bioceramics
Additive Manufacturing
Casting
MEMS

ABSTRACT

Polymer-derived ceramics exhibit excellent properties and are compatible with many shaping techniques due to their liquid precursors. We present a fast and pressureless process for the fabrication of SiCN. Using varied amounts of the filler divinyl benzene, defect-free monolithic disc samples are obtained at high yields. Their electrical conductivity is adjustable across 10 orders of magnitude, flexural strength is improved up to 1.7 GPa, and cytocompatibility is demonstrated. This processing route is applied to a new multiscale microshaping method combining the advantages of two-photon polymerization and casting. The parts' general shape is defined by KOH-etched silicon molds whereas individual freeform microfeatures like a 3D QR code are implemented through sacrificial 2PP photoresin microstructures added to the mold. The green body is pyrolyzed directly in the mold, whereby the photoresin decomposes and the ceramic part with the submicrometer resolution features imprinted releases itself from the mold undamaged due to ~30% shrinkage.

1. Introduction

Polymer-derived ceramics (PDCs) are a unique class of materials known for their resistance to high temperatures and harsh environments, property tunability, and compatibility with various shaping techniques [1]. Liquid silicon-containing preceramic polymers such as polysilazanes and polysiloxanes can be mixed with fillers, catalysts, or initiators in order to adapt them for shaping processes such as fiber drawing [2,3], coating [4,5], casting [6–9], or additive manufacturing. For the latter, polysiloxane-based formulations are typically prepared with photo initiators, fillers such as acrylates, UV absorbers, or solvents. Selective curing by light-exposure is mostly performed in commercial 3D printing systems, either by stereolithography (SLA)/digital light processing (DLP) for mesostructures [10,11], 2PP[1] for microstructures [12] or a combination of both for hierarchical multiscale structures [13]. These qualities make PDCs a versatile material with potential for different fields of application such as chemical engineering, energy conversion, and biomedical implants.

20–30 years ago, in the early stage of silicon carbonitride (SiCN) and silicon oxycarbide (SiOC) fabrication based on the PDC-route, the preceramic polymers were typically milled to powders after crosslinking. These were then pressed into powder compacts under high pressure, e.g. by hot isostatic pressing. Subsequent pyrolysis transforms the organic green body to ceramic material [14–17]. Alternatively, pressure-assisted direct processing of the liquid precursor was investigated, typically applying special pressure vessels and long curing times of several hours at elevated temperatures [6,8,18]. Only very few results on entirely pressureless bulk PDC processing have been published, typically based on curing of a polysiloxane and photoinitiator mixture by UV-irradiation [19,20].

For thermal crosslinking of polysilazanes, peroxides, mainly dicumyl peroxide (DCP), have been commonly used to reduce the curing temperature [21–23]. Many different kinds of fillers, added to the preceramic polymer, have been used in order to reduce shrinkage [24],

* Corresponding author.
E-mail addresses: lorenz.hageluken@epfl.ch (L. Hagelüken), juergen.brugger@epfl.ch (J. Brugger).

[1] The terms two-photon polymerization, microstereolithography, and (2PP-)direct laser writing (DLW) are sometimes used as synonyms, the abbreviation 2PP is used in the following only.

https://doi.org/10.1016/j.jeurceramsoc.2021.12.044
Received 4 October 2021; Received in revised form 7 December 2021; Accepted 16 December 2021
Available online 17 December 2021
0955-2219/© 2021 The Author(s). Published by Elsevier Ltd. This is an open access article under the CC BY-NC-ND license (http://creativecommons.org/licenses/by-nc-nd/4.0/).

create a controlled porosity [25], or tune the PDCs' composition and properties [26,27]. For instance, increase of the ceramics' carbon content and electrical conductivity have been achieved by the addition of divinyl benzene (DVB) [6,7].

Mechanical and functional properties of PDCs depend on their composition, microstructure, and integrity which are controllable through the choice of the polymeric precursor, additives, and processing parameters. Suitability for exposure to high temperatures [28] and harsh environments [29] has been shown. In addition to PDCs' electrical conductivity tuning, mechanical performance has been studied [18] and cytocompatibility was reported [27,30,31].

The liquid nature of the precursors and the cracking risk of larger bulk samples due to outgassing during pyrolysis [1] make PDCs the perfect candidates for part miniaturization and MEMS applications. High-aspect ratio structures and feature sizes down to 200 nm have been produced either by direct photolithography [9,32,33], 2PP [12,13,34], or replication of lithography-fabricated molds. Both hard and soft molds have been used for PDC microcasting, fabricated by deep reactive ion etching (DRIE) of silicon [30] or by photolithography of SU-8 [35] followed by polydimethylsiloxane (PDMS) replication of a thereby produced negative hard master [9,36], respectively.

In order to obtain defect-free SiOC and SiCN parts, long processes (hours up to days) utilizing pressure vessels or large presses are normally required. The related effort and cost have detrimental effects on the commercialization of PDCs. Furthermore, with respect to part shaping, a tradeoff between design freedom and cost exists as well. 2PP of preceramic polymers is time consuming and costly for large sample sizes or large sample numbers. High-precision microcasting on the contrary is very cost-effective but lacks the possibilities for customization.

In order to overcome these limitations, we present here a process for fast, pressureless fabrication of fully dense silicon carbonitride exhibiting very high yields, strength, tunable electrical conductivity, and cytocompatibility. A new hierarchical microfabrication process combines the advantages of 2PP and casting. Individual freeform microfeatures are implemented through the addition of custom sacrificial photoresin microstructures inside each mold whereas the parts' general shape is defined by a silicon mold.

2. Materials and methods

2.1. Mold fabrication and patterning

For PDC disc fabrication, custom-made CNC machined PTFE molds were used. Each mold contains 18 identical cylindrical cavities of 7 mm diameter and 500 μm depth.

Smaller molds were made by KOH-etching of silicon. For this, a 2 μm thick SiO_2 layer was thermally grown on 100 mm ⟨100⟩ Si wafers and subsequently patterned by photolithography and plasma etching, typically with rectangular shapes ranging from 1 to 20 mm in lateral size aligned to the primary flat. The patterned SiO_2 layer serving as a mask, Si molds were etched for 180 min in KOH (23%, 80 °C), until a depth of ~300 μm was reached. Removal of the SiO_2 was performed by hydrofluoric acid (HF) etching. The Si wafers were cut into 25 × 25 mm^2 dices, each containing 1–15 molds.

Freeform micropatterning was performed by 2PP (Photonic Professional GT+, Nanoscribe, Germany), using DiLL configuration with the 25× lens and IP-S resin. Micropatterns were written on the Si mold bottom, developed in propylene glycol methyl ether acetate and rinsed in isopropyl alcohol (IPA). A UV post curing was performed for 5 min (λ = 375 nm). Si molds and micropatterns were coated with 1 μm of Parylene-C by chemical vapor deposition (C-30-S, Comelec, Switzerland).

2.2. Synthesis of SiCN Ceramics

PDC-precursor formulation was performed in an Ar atmosphere glove box as summarized in Fig. 1. The poly(methylvinyl)silazane (PMVS) *Durazane*® 1800 has been provided by Merck KGaA, Germany. In each formulation, 3 wt.% of the radical initiator dicumyl peroxide (99%, Acros, United Kingdom) were added and dissolved. Subsequently, 0, 20, 40, or 60 wt.% DVB (80%, Sigma–Aldrich) were added. Formulations were stored in an inert, dark, and refrigerated place until casting, not later than 14 days after preparation.

PTFE molds were placed on a level hot plate inside the glove box. To compensate for partial volatilization, 23.1 μL of the precursor formulation (corresponding to 120% of a molds' volume) were pipetted into each mold, temporarily forming a convex liquid surface. Two upside-down glass beakers of different size were placed on top to create an oven-like thermally insulated chamber. Thermal crosslinking was performed during 30 min at 200 °C for 0% DVB formulations and in a 3-step process (10 min each at 100, 150, 200 °C) for the DVB-containing ones. Obtained green body material was released from the mold undamaged by upside-down tapping.

Si micromold casting was conducted in a similar way. By pipetting, DVB-free precursor formulation (120% of the respective mold volume) was added into each mold and crosslinking was performed during 20 min at 200 °C. Infusible material remained inside the mold for polymer-to-ceramic transformation.

Pyrolysis was conducted in a tube furnace (STF 15/450, Carbolite Gero, Germany) with a constant Ar flow. Green body discs and Si molds filled with the cured precursor were placed in alumina crucibles which were positioned in the furnace center. Heating and cooling rates of 100 K/h were applied, with a 1 h crosslinking dwell time at 300 °C and 1 h dwell time at the maximum temperature of 800, 1000, 1200, or 1400 °C.

2.3. Characterization

Part inspection and imaging were performed by optical microscopy (M80, Leica, Germany). A selection of 13 PDC disc samples was imaged by X-ray micro-computer tomography (Ultratom μCT system, RX-SOLUTIONS, France; 110 kV LaB^6 cathode).

Measurements and calculations of FTIR, TGA, DSC, Raman spectroscopy, flexural strength, and electrical conductivity were performed as reported previously [7]. For elemental analysis, up to three samples were manually ground to a fine powder and split into two fractions of approximately 5 mg for each of the five different sample types. One fraction was used in CHN(S) mode, the other one for oxygen analysis (Unicube, Elementar Analysensysteme, Germany). Si concentration was calculated as the difference to 100%. High-resolution imaging was done by SEM (Merlin, Zeiss, Germany).

Cytocompatibility of the PDCs was evaluated with normal human dermal fibroblasts (NHDF, PromoCell, cat. C12302, Lot 410Z037.5). Cells were cultured and maintained under standard cell culture conditions (37 °C, 5% CO_2, >95% humidity, in Dulbecco's modified minimal medium (DMEM) with high glucose, supplemented with 10% fetal calf serum (FCS), 1% penicillin–streptomycin–neomycin (PSN), and 1% L-glutamine). PDC disc samples doped with 20% and 40% DVB, each pyrolyzed at 1000 and 1200 °C, were sterilized by steam autoclaving (121 °C, 2 bar for 30 min). They were then placed upside-down in a 96-well plate and seeded with cells in 200 μL medium at ~15,500 cells/cm^2 on top. PDCs prepared without addition of DVB were used as reference. At days 1 and 4, metabolic activity of the cells was assessed with an MTS assay (Promega), according to the manufacturer's instructions. Absorbance was measured at 490 nm (Mithras2 plate reader, Berthold Technologies) with three technical repeats from triplicate samples per condition and time point. Cell attachment and spreading was observed by staining for the nuclei and cell cytoskeleton at day 1 and 4 after fixing and permeabilizing the cells with 4% paraformaldehyde and 0.1% Triton X-100 in PBS, respectively. After washing in PBS (3 times), cells were stained with Alexa Fluor 488 labelled phalloidin (Invitrogen, A12379) at a dilution of 1:200 (in 1X PBS) and DAPI (4,6-diamidino-2-

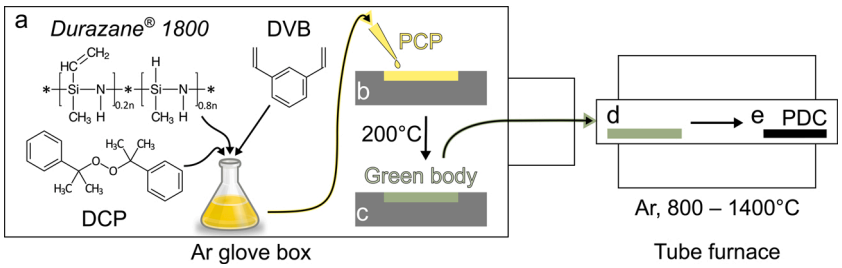

Fig. 1. Schematic of the PDC fabrication process in argon atmosphere: (a) precursor formulation, (b) casting and thermal crosslinking, (c) solidification and green body mold release, (d) green body transfer into tube furnace for pyrolysis, (e) transformation to PDC.

phenylindole, Sigma, D9542) at a dilution of 1:1000 (in 1X PBS) for 1 h. After washing with PBS, cells were imaged using a confocal laser scanning microscope (LSM 780, Carl Zeiss). Statistical analyses were performed using IBM SPSS statistics software (version 25). Error bars represent standard deviation. Data was analyzed using a Welch test with post-hoc Games Howell test when homogeneity of variances is not obeyed, with statistical significance defined at $p < 0.05$.

3. Results and discussion

3.1. PDC property tuning

An overview for the pressureless fabrication process of mm-sized SiCN discs is presented in Fig. 1. The poly(methylvinyl)silazane *Durazane 1800* can be crosslinked thermally without catalysts or initiators. The occurrence of the four crosslinking mechanisms which are shown in Fig. 2a is well known. Hydrosilylation is reported to occur above 100–120 °C, transamination in the range 200–400 °C, dehydrogenation above 300 °C, and vinyl polymerization at higher temperatures [37]. One of the main goals of our work was to find a new combination of precursor system and processing parameters in order to result in high-yield and high-quality samples in a short time, with a reduced need of large and expensive equipment such as presses. Rapid and pronounced crosslinking is targeted, to be achieved by the appropriate type and concentration of initiator as well as curing conditions. At the same time, mold damage, sample cracking, excessive mass loss, and pore formation caused by PTFE thermal decomposition, thermal stress, oligomer volatilization, and volatile trapping, respectively need to be avoided. For this reason, the radical initiator DCP was introduced at a comparably high concentration of 3 wt.%. DCP reportedly lowers the curing temperature of polyvinylsilazanes to 50–150 °C through initiation of the vinyl polymerization mechanisms [23,38]. In contrast to transamination and dehydrocoupling, vinyl polymerization is a mass-conservative mechanism and hence beneficial for achieving higher ceramic yields. In a similar way, in order to modify the composition and tune the properties, the carbon-filler DVB which was added to the preceramic polymer at four different concentrations of 0, 20, 40, and 60 wt.% is initiated by the DCP radicals. Activation of the vinyl group triggers the DVB polymerization and therefore supports the integration of DVB monomers and formed oligomers into the polysilazane crosslinking network. Without DVB addition, a 30 min heat treatment at 200 °C resulted in an adequate degree of thermosetting and absence of trapped bubble formation. For DVB-filled precursors, in order to reduce the DVB volatilization, a 3-step sequence of 10 min each at 100, 150, and 200 °C was applied, also leading to bubble-free disc green bodies as shown in Fig. 3a. Obtained green body samples are colorless and transparent in absence of DVB and become gradually more yellow and opaque with increasing DVB concentration. In case of the maximum DVB

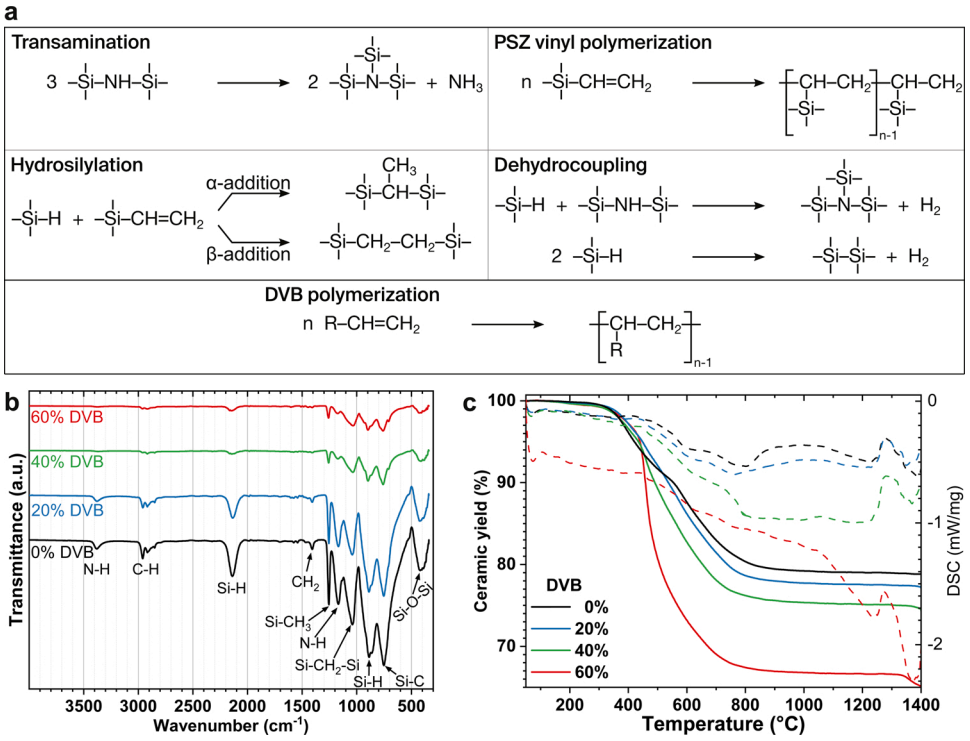

Fig. 2. (a) Polysilazane and divinyl benzene polymerization and crosslinking mechanisms; (b) FTIR spectra for each green body type exhibit the identical characteristic bands with decreasing intensity for increasing DVB amount; (c) TGA (solid) and DSC (dashed lines) performed in Ar: 0–40 wt.% DVB: slightly decreasing ceramic yields (79–75 wt.%) with increasing DVB concentration, 60 wt.% DVB: significantly lower value of 65 wt.% indicates reduced degree of crosslinking. DSC curves' minima show some exothermic reactions.

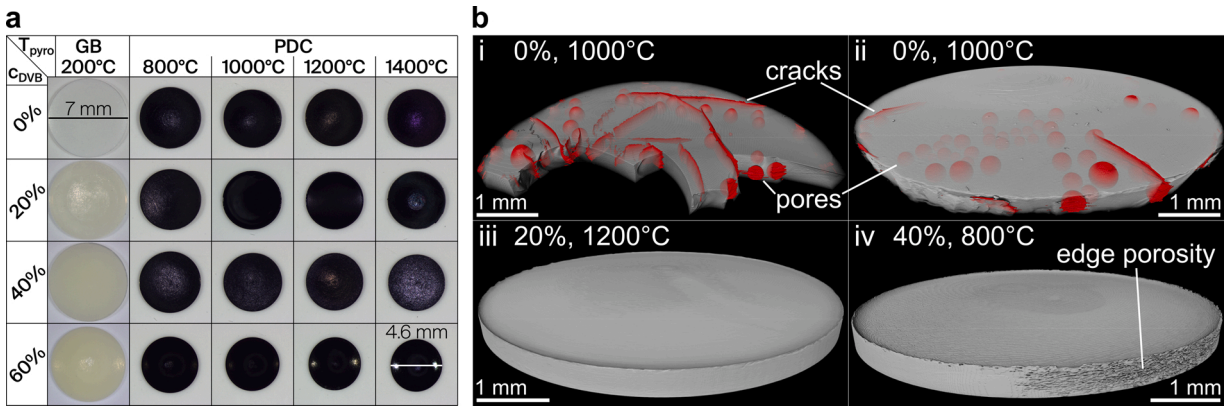

Fig. 3. Sample imaging: (a) Photographs of green body discs with four different DVB concentrations (in wt.%) and corresponding SiCN ceramic discs after argon pyrolysis at four different peak temperatures. Representation to scale visualizes the trend of higher shrinkage with increasing DVB concentration and increasing pyrolysis temperature; (b) microtomography images of four PDC disc samples with cracks and pores highlighted in red: (i,ii) 0% DVB 1000°C before process optimization suffering from severe pore and crack formation; (iii) 20% DVB 1200 °C with optimized processing leads to best results, fully dense samples without any noticeable pore or cracks; (iv) optimized 40% DVB 800 °C exhibits no enclosed pores or cracks but some minor edge porosity. (For interpretation of the references to color in this figure legend, the reader is referred to the web version of this article.)

concentration of 60 wt.%, slight warping is observed already in the green body state.

Fourier-transform infrared spectroscopy (FTIR) data of the four different green body samples shown in Fig. 2b does not exhibit bands related to the vinyl group stretching (ν_{C-H} at 3053 cm^{-1}, $\nu_{C=C}$ at 1592 and 1402 cm^{-1}) [39], confirming their complete consumption. Various bands of the polysilazane's other functional groups such as N—H at 3378 cm^{-1} and Si—H at 2118 cm^{-1} persist, indicating overall incomplete crosslinking of the system after the first thermal treatment. For this reason, a 1 h 300 °C dwell time was included in the subsequent argon pyrolysis process, allowing transamination and dehydrocoupling to proceed. Thermogravimetric analysis (TGA) of the same samples in Fig. 2c illustrates the polymer-to-ceramic transformation process. All compositions behaved very similarly up to 440 °C where the organic-inorganic transition sets in and the 60% DVB formulation exhibits a severe mass loss. This extra mass loss of 10% indicates an excess amount of DVB, unable to integrate into the polymeric network and hence decomposing and volatilizing. For DVB concentrations of 20 and 40 wt.%, however, the filler is mostly incorporating into the network. Therefore, high ceramic yields of 77% and 75% were acquired at 1400 °C, which is only slightly below the value of 79% for the DVB-free material.

Pyrolysis of the green body discs was conducted in an argon flow at low heating and cooling rates of 100 K/h in order to reduce the risk of cracking due to thermal stress. Fig. 3a shows one example of each obtained PDC sample type after pyrolysis. Relative shrinkage ranged from 24% to 36% laterally (diameter) and 7% to 48% vertically (thickness). As a general trend, increasing shrinkage was observed with higher DVB concentrations and higher pyrolysis temperatures. This can be explained with ongoing material densification, mainly through hydrogen stripping in remaining C—H bonds [1].

Defects such as unintentional pore formation, cracking or severe warping are common problems in PDC fabrication. Our optimized precursor system and processing parameters in contrast allow for a very reliable and predictable sample fabrication. Among nearly 800 PDC disc samples produced, less than 1% exhibited visible pores or cracks. In order to reveal potential internal defects, X-ray microtomography scans of 13 samples were performed. In Fig. 3b, two examples are shown where the DCP concentration was only 2 wt.% and a higher temperature curing sequence (200–250 °C) was applied. A large number of trapped bubbles is present in both samples i and ii, that already formed during the first thermal treatment step and were conserved during the subsequent thermal processing. Tearing cracks may already occur in the green body state but, similar to the full fracture in sample i, they are typically the consequence of rapid heating and cooling during the pyrolysis. Due to overpressure formed in enclosed pores or thermal stress related to temperature gradients in the material, cracks are formed, in particular along pores. Our process modifications reliably allowed avoidance of such defects as samples iii and iv in Fig. 3b show, as well as ii–ix in Fig. S1. The obtained ceramic material is fully dense, however, with some artefacts present. Due to the liquid precursor casting approach and minor volatilization during crosslinking, samples tend to form a meniscus at the top side edge which is more pronounced at higher DVB concentrations (Fig. S1 viii, ix). In case of 40% DVB filling, some micro edge porosity formed (Figs. 3b iv and S1 vii, viii), probably caused by pinning of evolving gas at the mold side wall. The maximum DVB concentration of 60wt.% causes the green body to warp, an effect which becomes even more pronounced after pyrolysis (Fig. S1 iii).

Polysilazanes are precursors for silicon carbonitride (SiCN) which is obtained as a so-called amorphous covalent ceramic (ACC) with mixed bonds after pyrolysis in an inert atmosphere [40,41]. The amorphous character of the obtained PDCs has been verified by X-ray diffraction (data not shown). In order to determine the composition, five sample types were selected and respective disc samples were ground to a fine powder and analyzed by elemental analysis (EA). 1000 °C pyrolyzed samples of all four precursor compositions were chosen as well as a second 20% DVB sample but pyrolyzed at 1400 °C. This way, both DVB concentration and temperature influence can be seen. The resulting carbon, nitrogen, hydrogen, and oxygen concentrations for each sample are listed in Table 1, where the silicon concentration was calculated as the difference to 100%. Conversion to the empirical formulae normalized to Si_1 shows that the oxygen contamination is negligible (<0.006 mol). The samples' free carbon content was calculated based on a set of atomic bonding assumptions according to the literature [42,43]. Due to the organic character of the used PMVS resulting ceramic material contains a significant inherent carbon concentration of 21 wt.%. This value is in good agreement with a similarly prepared PDC from the literature [44]. Subtracting the approximate C atoms bonded to hydrogen and silicon gives the approximate fraction of "free" sp^2-hybridized carbon which is 15 wt.% in this case. In general, free-carbon incorporation is of interest because of positive influences on the PDCs' properties such as improved thermal stability and establishment of a metallic-like electron conduction [1]. Addition of 20 and 40 wt.% DVB to the precursor was proven to be effective as the corresponding free carbon values in the resulting ceramic increase by 5 wt.% each, to a maximum of 25 wt.%. Higher values of up to 55 wt.% have been reported but required more complex or time-consuming processing [43,45]. In agreement with the observations on 60 wt.% DVB addition

Table 1
Selected PDC samples' elemental composition, empirical formulae normalized to Si_1, and calculated free carbon content. A maximum free carbon content of 24.9% is observed for 40% DVB.

#	c_{DVB} (wt.%)	T_{pyro} (°C)	Elemental content (wt.%)					Empirical formula	Free carbon (wt.%)
			Si	C	N	H	O		
1	0	1000	56.5	21.3	20.8	1.3	0.12	$SiC_{0.88}N_{0.74}H_{0.64}$	14.5
2	20	1000	52.1	27.1	19.9	0.90	0.06	$SiC_{1.22}N_{0.77}H_{0.48}$	20.3
3	20	1400	53.1	27.8	18.8	0.26	0.05	$SiC_{1.23}N_{0.71}H_{0.14}$	18.0
4	40	1000	48.5	30.8	20.0	0.67	0.03	$SiC_{1.48}N_{0.83}H_{0.38}$	24.9
5	60	1000	52.1	31.4	15.8	0.48	0.17	$SiC_{1.41}N_{0.61}H_{0.25}$	20.8

described before, such a high filler concentration gives inferior results with a free carbon concentration of only 21 wt.%, comparable to the value of 20% DVB. Comparing the two EA measurements of 20% DVB confirms the expected trend of mainly hydrogen stripping occurring in the temperature range of 1000–1400 °C.

Raman spectroscopy is a powerful non-destructive method for carbonaceous materials structure analysis. Measured spectra of all 16 PDC sample types presented in Fig. 4a exhibit two bands at ~1350 and 1600 cm^{-1}, called D and G band, respectively. The D band is caused by the free carbon's disorder-induced vibration mode of graphene-like sp^2-rings. In-plane bond stretching of sp^2-hybridized carbon atoms is responsible for the G band [44,46]. Lorentzian peak fitting of the baseline-subtracted spectra was performed in order to determine both bands' intensities, peak position, and full width at half maximum (FWHM). The increasing I_D/I_G intensity ratio of all four compositions with increasing pyrolysis temperature as well as the D band width decrease indicate a carbon ordering towards aromatic graphene layers proceeding in the temperature range of 800–1400 °C [44,46]. Details are shown for the set of 20% DVB containing samples in Fig. S2.

This carbon ordering process is one reason for the observed large range in electrical conductivity of 10 orders of magnitude. Samples with 0% and 20% DVB added were found to be insulating with 4.6×10^{-11} and 3.7×10^{-9} S cm^{-1} as lowest and highest conductivity values measured, respectively. A maximum free carbon content of 20 wt.% in those samples appears to be insufficient for the establishment of a carbon percolation network which is reported to be mainly responsible for electrical conductivity in SiCN [1]. A major conductivity increase is observed when increasing the amount of added DVB to 40%, resulting in approximately 25 wt.% of free carbon in the obtained ceramic, which appears to be above the threshold concentration. 40% DVB samples pyrolyzed at 800 °C exhibit a conductivity of $\sim 8.4 \times 10^{-7}$ S cm^{-1}. With an increasing pyrolysis temperature samples of this composition become constantly more conductive up to metallic-like 0.4 S cm^{-1}, with a maximum measured value of 1.3 S cm^{-1}. This trend is in line with previous investigations [6,7] and is caused by hydrogen stripping and the sp^3-to-sp^2 transition described before [1]. Data acquired for 60% DVB samples is less reproducible and has larger variation, which is another sign for this composition's poor qualities. The complete data set of measured electrical conductivity values is provided in Table S1 and should be considered as a basis for the above described trends only since it was derived from single samples.

Mechanical performance of twelve sample types (0–40% DVB, 800 °C < T_{pyro} < 1400 °C) was investigated by means of ball-on-three-balls (B3B) testing of SiCN discs. 60% DVB samples were excluded due to shrinkage and excessive warpage. Calculated flexural strength values of three tested samples each are summarized in Table S2. Typical for ceramics, presence of hidden defects may cause large variation of results such as in the case of 0% DVB 1200 °C ranging from 77 up to 1350 MPa. Hence, based on this data set, two sample types have been chosen for repeated testing with 12–15 samples each. The results of 1000 °C pyrolyzed samples with 20% and 40% DVB added to the precursor formulation are presented in Fig. 4b as a Weibull plot. The derived characteristic flexural strength value of 988 MPa for the 40% DVB composition is comparable to results we have obtained recently for similarly measured DVB-modified SiOC [7]. In contrast, the flexural strength of 20% DVB modified SiCN of 1.7 GPa is outperforming previously published results for PDCs with maximum values of 1.1 GPa [1,18,47]. Considering the Weibull modulus also being significantly higher for 20% DVB than 40%, the lower DVB addition is clearly favorable for mechanically demanding applications. The differing behavior of these two sample types may be explained by the 20% DVB samples' naturally smoother top surface, absence of edge microporosity, and possibly lower internal micro flaw concentration, [47] rather than by the actual composition.

In order to evaluate the PDCs' suitability for biomedical applications, their cytocompatiblity was assessed with human dermal fibroblasts (NHDF). For this, NHDF were cultured for 1 and 4 days on the bottom surface of the disc samples and metabolic activity as well as cell attachment and spreading on the substrate were investigated for samples with 0%, 20%, and 40% DVB added (pyrolyzed at 1000 and 1200°C). Confocal microscopy shows well spread cells with no obvious differences on all PDC groups at day 1 (Fig. 5a). After 4 days of culture, a

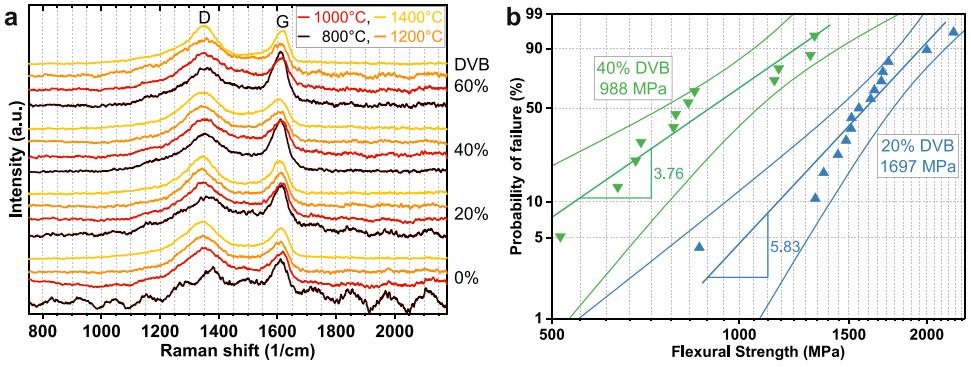

Fig. 4. PDC characterization: (a) Raman spectroscopy of all 16 sample types where the free carbon D and G band intensity ratio indicates the ordering; (b) Weibull diagram of two best performing sample types which are 1000 °C pyrolyzed 20% and 40% DVB, exhibiting flexural strength values of 1.7 GPa and 988 MPa, respectively.

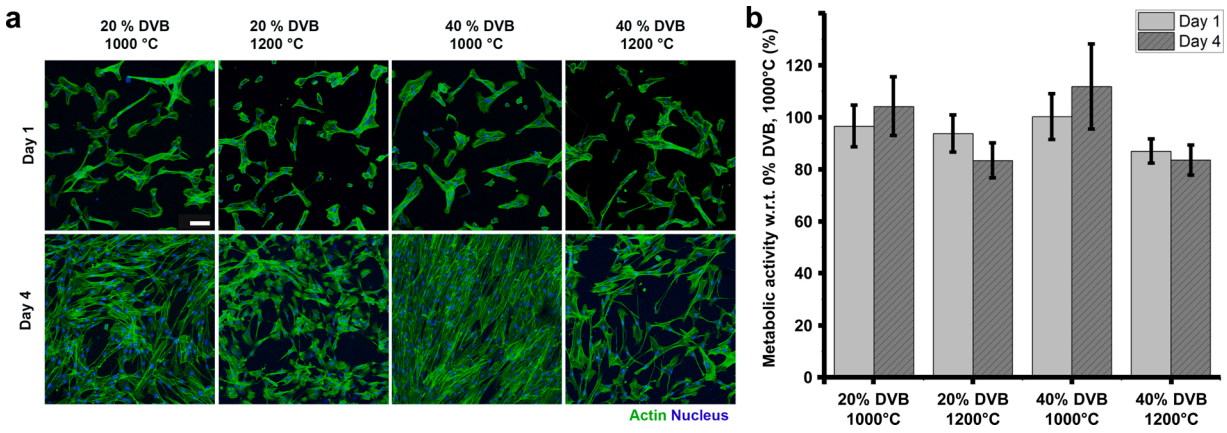

Fig. 5. Cytocompatibility of four different SiCN sample types: (a) representative confocal images of cells on the surface of PDCs, stained for actin (green) and nucleus (blue) at day 1 and 4, scale bar: 100 μm; (b) NHDF on the surface of PDCs with metabolic activity quantified by an MTS assay ($N = 3$). (For interpretation of the references to color in this figure legend, the reader is referred to the web version of this article.)

cell layer was observed on PDCs pyrolyzed at 1000 °C, while less cells were visible on PDCs pyrolyzed at 1200 °C. Quantification of the cells' metabolic activity (Fig. 5b) did not show significant differences between the conditions at day 1, reflecting the observation in the images. At day 4, the metabolic activity of cells on PDCs pyrolyzed at 1200 °C showed slightly lower levels than cells grown on substrates pyrolyzed at 1000 °C, but differences are not statistically significant. While this indicates that elevated pyrolysis temperatures might alter surface properties, which in turn affects cell attachment and proliferation, further research would be needed. Importantly however, the increased carbon concentrations to improve the mechanical and electrical properties do not affect cell attachment nor their metabolic activity, which is in agreement with previous reports where DVB was used in a similar way [30]. Collectively, the data presented here shows the cytocompatibility and thus the suitability of DVB as an additive that improves the mechanical and electrical properties of PDCs for biomedical applications.

3.2. Multiscale microfabrication

In addition to the mm-size disc shaped SiCN samples fabricated for material testing, the same process route was applied to casting of microsized PDC parts. To this end, silicon hard molds were made by anisotropic potassium hydroxide (KOH) wet etching and directly used to define the ceramic parts' general shape. The alternative dry etching of Si such as the Bosch process gives approximately vertical sidewalls but suffers from detrimental effects such as convex mold bottoms, micrograss formation, and scalloped sidewalls [48–50]. In contrast, KOH etching of ⟨100⟩ silicon yields 54.7° angled sidewalls, flat mold bottoms, and very smooth surfaces. Such structures are shown in Fig. 6a comprising ~300 μm deep molds of 5 × 5, 10 × 10, and 20 × 20 mm^2 lateral size. These may be used directly for casting of the preceramic polymer formulation. A CVD deposition of 1 μm Parylene-C, however, was found to improve the part release behavior.

In order to introduce additional microfeatures with free form capabilities and part customization, 2PP has been performed on the KOH Si

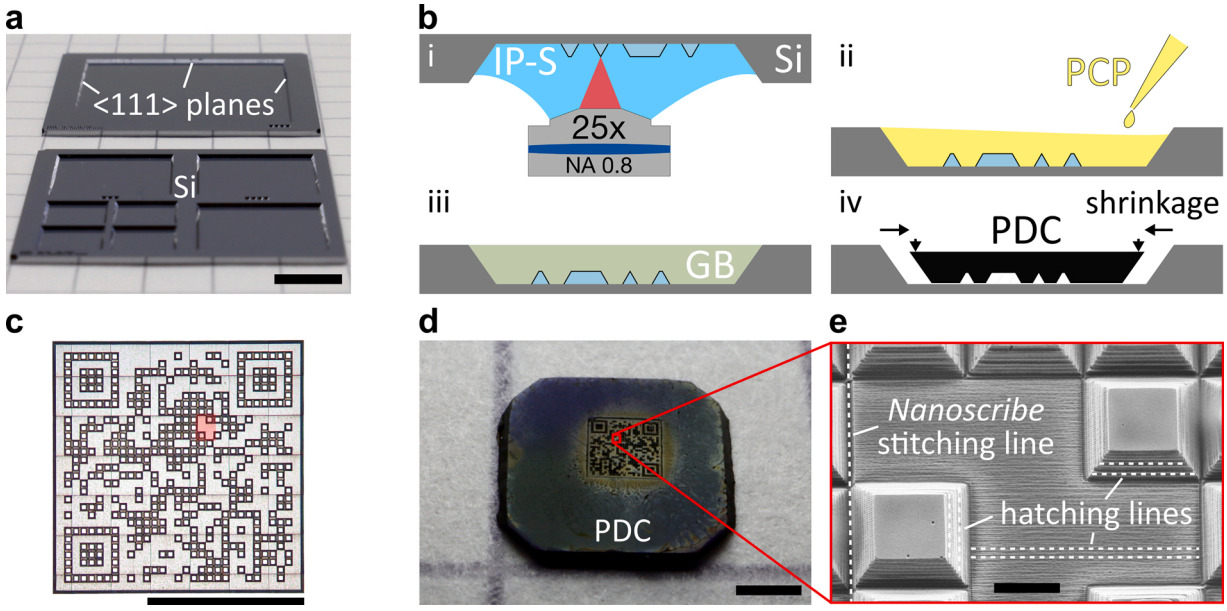

Fig. 6. Multiscale PDC microfabrication: (a) KOH-etched Si chips with 300 μm deep molds of 5 × 5, 10 × 10, and 20 × 20 mm^2 lateral size; (b) process flow: (i) upside-down 2PP on mold bottom, (ii) PCP casting, (iii) thermal conversion to GB state, (iv) shrunk sample with feature imprint after pyrolysis; (c) optical micrograph of a 2PP inverted QR code with mesa pixels and ROI highlighted; (d) pyrolyzed PDC part with the QR code imprinted; (e) SEM close-up view at the PDC QR pixels. Scale bars: a: 5 mm, c and d: 1 mm, e: 20 μm.

mold bottoms. This process is summarized in Fig. 6b. Using a commercial 2PP system and photoresin IP-S (*Nanoscribe GmbH*), mm-sized polymeric structures were added onto the mold bottom by IP-S drop casting, selective microstereolithography 2PP-crosslinking (i), and development. This particular resin is intended for smooth surfaces at the micro- and mesoscale. UV post curing and Parylene-C deposition were performed in order to render the modified mold more resilient and improve the part release. In an analogous manner to the disc casting in PTFE described before, the PMVS-based formulation (3 wt.% DCP, no DVB) was pipetted into the mold (ii). To compensate for partial volatilization during curing, again 120% of the molds' theoretical volume were used. Unlike other reports on microcasting of preceramic polymer [35,36] no pressure was applied for thermal curing. A short 20 min heating at 200 °C in an Ar glove box is sufficient in this case to give infusible material free of cracks and bubbles (iii: GB) which can safely be transferred into the furnace for pyrolysis. Similar to Liew et al. [35], the samples were not demolded before pyrolysis but remain inside the mold for polymer-to-ceramic transformation. This way damaging of the fragile green bodies can be avoided. Unlike their SU-8 frame which decomposes, the Si mold in our case survives the thermal treatment at 1000 °C undamaged and only the IP-S 3D structure decomposes. Due to the Parylene-C separation layer and the GB's lateral shrinkage of ~27% the PDC part is obtained loose and undamaged in the mold after process completion (iv).

Several 2PP microstructures have been realized such as a 3D Quick Response (QR) code, presented in Fig. 6c. It is the negative of 50 × 50 μm^2 sized square mesa pixels with a height of 12.5 µm and lateral total dimensions of 1.65 × 1.65 mm^2, written in 49 stitching blocks of 250 × 250 μm^2 each. The QR code represents the URL of our lab website. During the pyrolysis sequence, both the Parylene-C layer and acrylic-based IP-S structure decompose with the majority of the products outgassing. A very small amount of glassy carbon remains, 2–10% for the photoresin and ~35% of the Parylene-C [51–53]. The infusible preceramic polymer adopts the respective mold and 3D microstructure shape, which is conserved during the polymer-to-ceramic transformation occurring shortly after the decomposition of the other two materials. As a result, the 2PP 3D structure is imprinted mirror-inverted on the bottom side of the PDC part (Fig. 6d). The cavity pixels from the print correspond to the mesa pixels extruded from the new recessed base level. The PDC part is free of cracks and pores but as a consequence of the decomposition outgassing, radially oriented traces are visible. Fig. 6e shows an SEM image of the region highlighted in red in c and d. The replication of the 2PP structure is very precise. The liquid precursor formulation filled the mold conformly and no bubbles were trapped or formed, showing that neither vacuum degassing nor pressure-assisted curing are necessary. Even printing artefacts such as stitching and hatching lines (~750 nm) are clearly visible, showcasing the submicrometer PDC-replication capability which we have demonstrated for simpler tip-geometries before [54]. The PDC mesa pixel top surfaces which were in direct contact with the Parylene-C coated silicon area are noticeably smoother than the now recessed bottom area. No contamination from the IP-S photoresin derivatives in the form of glassy carbon particles remains after rinsing the sample with IPA. Occurring shrinkage during the polymer-to-ceramic transformation can either be exploited for higher resolution or compensated in the design phase.

This example shows the feasibility of our hierarchical PDC shaping technique. Differently sized and shaped Si molds can be applied alternatively, also as 2.5D multilayer molds with subsequent etching steps and angled (KOH) or vertical (Bosch) sidewalls or a combination of them. When reusing the Si molds, effective part fabrication cost can be kept at a reasonable level due to the fast and reliable character of the process and reduced need of special hardware. Definition of the general shape by the mold and application of 2PP only where needed shortens the printing time and hence reduces cost further compared to 2PP-writing of the entire (pre)ceramic part. In addition to any kind of part labelling, protection against forgery, surface patterning and functionalization such as altering hydrophobicity, or 2D and 3D microfluidic structures can be realized this way in ceramic.

4. Conclusions

This paper describes a facilitated process for the high-yield fabrication of fully dense poly(methylvinyl)silazane-derived silicon carbonitride. Due to the thermal initiator dicumyl peroxide, the preceramic polymer was thermally cured at a moderate temperature of 200 °C at ambient pressure in only 30 min. The addition of the carbon filler divinyl benzene modified the composition of the PDC obtained after pyrolysis, i.e. the free carbon content in the range 15–25 wt.%, which was verified by means of elemental analysis. Crosslinking behavior was monitored by FTIR spectroscopy and ceramic yields up to 79% were observed in TGA measurements. As analyzed by µ-tomography, defect-free samples were fabricated, whose structure, mechanical, and electrical behavior have been investigated. DVB additions of 20 and 40 wt.% were found to be beneficial for achieving ceramics with very high flexural strength up to 1.7 GPa and maintained cytocompatibility. Metallic-like electrical conductivity up to 0.4 S cm^{-1} was observed in 40% DVB materials due to the increased free carbon content.

The presented process is compatible with a new multiscale microfabrication approach for PDCs. Mesoscale KOH-etched silicon molds with smooth surfaces were refined by freeform microfeature addition through 2PP. In a fast and pressureless preceramic polymer casting process, the shape defined by the multiscale mold has been successfully replicated into a PDC part with submicrometer resolution. Due to target-oriented application of 2PP and the option to reuse the Si mold part fabrication cost can be reduced.

The outstanding properties of polymer-derived silicon carbonitride such as high-temperature stability, chemical inertness, high strength, tunable functional properties, and cytocompatibility make this versatile material a valuable candidate for potential applications in various fields. In combination with the design freedom and resolution of the demonstrated multiscale microshaping technique use in chemical engineering, energy conversion, and especially biomedical implants should be considered.

Conflict of interest

None declared.

Declaration of Competing Interest

The authors report no declarations of interest.

Acknowledgements

This work was supported by the ETH domain, through the Strategic Focus Area (SFA) — Advanced Manufacturing program under the project named Ceramic X.0 — High-precision micro-manufacturing of ceramics. Valuable discussions with the staff of the EPFL Center of Micro/NanoTechnology (CMi) are appreciated. The authors thank *Kern Microtechnik GmbH* for providing the PTFE molds, Giuilia Panusa and Eirini Kakkava for performing the Raman spectroscopy, and Gary Perrenoud for performing the microtomography scans and help with their processing. *Durazane 1800* was provided by *Merck Performance Materials*.

Appendix A. Supplementary data

Supplementary data associated with this article can be found, in the online version, at https://doi.org/10.1016/j.jeurceramsoc.2021.12.044.

References

[1] P. Colombo, G. Mera, R. Riedel, G.D. Soraru, Polymer-derived ceramics: 40 years of research and innovation in advanced ceramics, J. Am. Ceram. Soc. 93 (2010) 1805–1837.
[2] S. Kokott, L. Heymann, G. Motz, Rheology and processability of multi-walled carbon nanotubes-ABSE poly carbosilazane composites, J. Eur. Ceram. Soc. 28 (2008) 1015–1021.
[3] O. Flores, R.K. Bordia, D. Nestler, W. Krenkel, G. Motz, Ceramic fibers based on SiC and SiCN systems: current research, development, and commercial status, Adv. Eng. Mater. 16 (2014) 621–636.
[4] J.D. Torrey, R.K. Bordia, Processing of polymer-derived ceramic composite coatings on steel, J. Am. Ceram. Soc. 91 (2008) 41–45.
[5] G. Barroso, Q. Li, R.K. Bordia, G. Motz, Polymeric and ceramic silicon-based coatings – a review, J. Mater. Chem. A 7 (2019) 1936–1963.
[6] F. Dalcanale, et al., Influence of carbon enrichment on electrical conductivity and processing of polycarbosilane derived ceramic for MEMS applications, J. Eur. Ceram. Soc. 34 (2014) 3559–3570.
[7] P.V.W. Sasikumar, et al., Polymer derived silicon oxycarbide ceramic monoliths: microstructure development and associated materials properties, Ceram. Int. 44 (2018) 20961–20967.
[8] L. An, W. Zhang, V. Bright, M. Dunn, R. Raj, Development of injectable polymer-derived ceramics for high temperature MEMS, Proceedings IEEE 13th Annual International Conference on MEMS (Cat. No.00CH36308) (2000).
[9] S. Martınez-Crespiera, et al., Fabrication of silicon oxycarbide-based microcomponents via photolithographic and soft lithography approaches, Sens. Actuators A: Phys. 169 (2011) 242–249.
[10] Z.C. Eckel, et al., Additive manufacturing of polymer-derived ceramics, Science 351 (2016) 58–62.
[11] E. Zanchetta, et al., Stereolithography of SiOC ceramic microcomponents, Adv. Mater. 28 (2016) 370–376.
[12] G. Konstantinou, et al., Additive micro-manufacturing of crack-free PDCs by two-photon polymerization of a single, low-shrinkage preceramic resin, Addit. Manuf. 35 (2020) 101343.
[13] J. Schmidt, et al., Multiscale ceramic components from preceramic polymers by hybridization of vat polymerization based technologies, Addit. Manuf. 30 (2019) 100913.
[14] R. Riedel, G. Passing, H. Schonfelder, R.J. Brook, Synthesis of dense silicon-based ceramics at low temperatures, Nature 355 (1992) 714–717.
[15] C. Konetschny, D. Galusek, S. Reschke, C. Fasel, R. Riedel, Dense silicon carbonitride ceramics by pyrolysis of cross-linked and warm pressed polysilazane powders, J. Eur. Ceram. Soc. 19 (1999) 2789–2796.
[16] S. Ishihara, H. Gu, J. Bill, F. Aldinger, F. Wakai, Densification of precursor-derived Si-C-N ceramics by high-pressure hot isostatic pressing, J. Am. Ceram. Soc. 85 (2002) 1706–1712.
[17] S. Trassl, M. Puchinger, E. Rossler, G. Ziegler, Electrical properties of amorphous SiCxNyHz-ceramics derived from polyvinylsilazane, J. Eur. Ceram. Soc. 23 (2003) 781–789.
[18] S.R. Shah, R. Raj, Mechanical properties of a fully dense polymer derived ceramic made by a novel pressure casting process, Acta Mater. 50 (2002) 4093–4103.
[19] S. Martınez-Crespiera, E. Ionescu, H.-J. Kleebe, R. Riedel, Pressureless synthesis of fully dense and crack-free SiOC bulk ceramics via photo-crosslinking and pyrolysis of a polysiloxane, J. Eur. Ceram. Soc. 31 (2011) 913–919.
[20] X. Yang, P. Jiang, F. Sun, L. Yang, X. Fan, A pyrolysis heating rate based pressureless method for preparing dense and crack-free polymer-derived silicon oxycarbide bulk ceramics, Ceram. Int. 46 (2020) 10392–10399.
[21] E. Kroke, et al., Silazane derived ceramics and related materials, Mater. Sci. Eng. R Rep. 26 (2000) 97–199.
[22] J. Wilfert, M. Jansen, Curing preceramic SiBNC polymers infusible by radical polymerization, J. Mater. Chem. 21 (2011) 13422.
[23] R. D'Elia, et al., Effect of dicumyl peroxide concentration on the polymerization kinetics of a polysilazane system, Polym. Eng. Sci. 58 (2017) 859–869.
[24] P. Greil, Active-filler-controlled pyrolysis of preceramic polymers, J. Am. Ceram. Soc. 78 (1995) 835–848.
[25] C. Vakifahmetoglu, et al., Highly porous macro- and micro-cellular ceramics from a polysilazane precursor, Ceram. Int. 35 (2009) 3281–3290.
[26] E. Ionescu, A. Francis, R. Riedel, Dispersion assessment and studies on AC percolative conductivity in polymer derived Si-C-N/CNT ceramic nanocomposites, J. Mater. Sci. 44 (2009) 2055–2062.
[27] P.V.W. Sasikumar, et al., In Vitro Cytocompatibility Assessment of Ti-Modified, Silicon-oxycarbide-based, polymer-derived, ceramic-implantable electrodes under pacing conditions, ACS Appl. Mater. Interfaces 12 (2020) 17244–17253.
[28] E. Ionescu, et al., Polymer-derived ultra-high temperature ceramics (UHTCs) and related materials, Adv. Eng. Mater. 21 (2019) 1900269.
[29] L.-A. Liew, et al., Processing and characterization of silicon carbon-nitride ceramics: application of electrical proper ties towards MEMS thermal actuators, Sens. Actuators A: Phys. 103 (2003) 171–181.
[30] J. Grossenbacher, et al., Cytotoxicity evaluation of polymer-derived ceramics for pacemaker electrode applications, J. Biomed. Mater. Res. Part A 103 (2015) 3625–3632.
[31] J. Jang, et al., Electrochemical performance of polymer-derived SiOC and SiTiOC ceramic electrodes for artificial cardiac pacemaker applications, Ceramics International, 2020.
[32] T. Cross, et al., Fabrication process for ultra-high aspect ratio polysilazane-derived MEMS. Technical Digest, 15th IEEE International Conference on MEMS (Cat. No.02CH37266) (2002).
[33] L.-A. Liew, et al., Fabrication of SiCN MEMS by photopolymerization of pre-ceramic polymer, Sens. Actuators A: Phys. 95 (2002) 120–134.
[34] J. Bauer, et al., Additive manufacturing of ductile, ultrastrong polymer-derived nanoceramics, Matter 1 (2019) 1547–1556.
[35] L.-A. Liew, et al., Fabrication of SiCN ceramic MEMS using injectable polymer-precursor technique, Sens. Actuators A: Phys. 89 (2001) 64–70.
[36] J. Grossenbacher, et al., On the micrometre precise mould filling of liquid polymer derived ceramic precursor for 300-µm-thick high aspect ratio ceramic MEMS, Ceram. Int. 41 (2015) 623–629.
[37] G. Mera, E. Ionescu, Silicon-Containing Preceramic Polymers. Encyclopedia of Polymer Science and Technology, 2013.
[38] Y. Li, et al., Thermal cross-linking and pyrolytic conversion of poly (ureamethylvinyl)silazanes to silicon-based ceramics, Appl. Organometall. Chem. 15 (2001) 820–832.
[39] D. Fonblanc, et al., Crosslinking chemistry of poly(vinylmethyl-co-methyl)silazanes toward low-temperature formable preceramic polymers as precursors of functional aluminium-modified Si-C-N ceramics, Dalton Trans. 47 (2018) 14580–14593.
[40] P. Greil, Polymer derived engineering ceramics, Adv. Eng. Mater. 2 (2000) 339–348.
[41] E. Ionescu, Ceramics science and technology, in: R. Riedel, I.-W. Chen (Eds.), Set, Wiley-VCH Verlag GmbH & Co. KGaA, Weinheim, Germany, 2013, pp. 457–500.
[42] G.D. Soraru, et al., Chemical durability of silicon oxycarbide glasses, J. Am. Ceram. Soc. 85 (2002) 1529–1536.
[43] G. Liu, J. Kaspar, L.M. Reinold, M. Graczyk-Zajac, R. Riedel, Electrochemical performance of DVB-modified SiOC and SiCN polymer-derived negative electrodes for lithium-ion batteries, Electrochim. Acta 106 (2013) 101–108.
[44] M. Graczyk-Zajac, C. Fasel, R. Riedel, Polymer-derived-SiCN ceramic/graphite composite as anode material with enhanced rate capability for lithium ion batteries, J. Power Sources 196 (2011) 6412–6418.
[45] L. Ribeiro, et al., The influence of pyrolysis temperature on the oxidation resistance of carbon-rich SiCN ceramics derived from reaction of silazanes with acrylonitrile, J. Eur. Ceram. Soc. 41 (2021) 3285–3291.
[46] A.C. Ferrari, J. Robertson, Interpretation of Raman spectra of disordered and amorphous carbon, Phys. Rev. B 61 (2000) 14095–14107.
[47] R. Sujith, S. Jothi, A. Zimmermann, F. Aldinger, R. Kumar, Mechanical behaviour of polymer derived ceramics – a review, Int. Mater. Rev. (2020) 1–24.
[48] J. Kiihamaki, Fabrication of SOI Micromechanical Devices (Ph.D. thesis), 2005, p. 87 [28].
[49] S.-B. Jo, et al., Characterization of a modified Bosch-type process for silicon mold fabrication, J. Vac. Sci. Technol. A 23 (2005) 905–910.
[50] K.-S. Chen, A. Ayon, X. Zhang, S. Spearing, Effect of process parameters on the surface mor phology and mechanical performance of silicon structures after deep reactive ion etching (DRIE), J. Microelectromech. Syst. 11 (2002) 264–275.
[51] A. Zakhurdaeva, et al., Custom-designed glassy carbon tips for atomic force microscopy, Micromachines 8 (2017) 285.
[52] Y. Liu, et al., Structural color three-dimensional printing by shrinking photonic crystals, Nat. Commun. (2019) 10.
[53] K.C. Morton, C.A. Morris, M.A. Derylo, R. Thakar, L.A. Baker, Carbon electrode fabrication from pyrolyzed Parylene C, Anal. Chem. 83 (2011) 5447–5452.
[54] J. Grossenbacher, M.R. Gullo, R. Grandjean, T. Kiefer, J. Brugger, Sub micrometer ceramic structures fabricated by molding a polymer-derived ceramic, Microelectron. Eng. 97 (2012) 272–275.